Physica D 471 (2025) 134432

Contents lists available at ScienceDirect

Physica D

journal homepage: www.elsevier.com/locate/physd

Energy localisation and dynamics of a mean-field model with non-linear dispersion

H. Christodoulidi [a], Ch. G. Antonopoulos [b,*]

[a] University of Lincoln, School of Mathematics and Physics, Brayford Pool Campus, Lincoln, LN6 7TS, UK
[b] University of Essex, School of Mathematics, Statistics and Actuarial Science, Wivenhoe Park, Colchester, CO4 3SQ, UK

ARTICLE INFO

Communicated by J. Cuevas-Maraver

Keywords:
Energy localisation
Lyapunov exponents
Quasi-stationary states
q-statistics

ABSTRACT

In this paper, we examine the dynamical and statistical properties of a mean-field Hamiltonian with on-site potentials, where particles interact via nonlinear global forces. The absence of linear dispersion triggers a variety of interesting dynamical features associated with very strong energy localisation, weak chaos and slow thermalisation processes. Particle excitations lead to energy packets that are mostly preserved over time. We study the route to thermalisation through the computation of the probability density distributions of the momenta of the system and their slow convergence into a Gaussian distribution in the context of non-extensive statistical mechanics and Tsallis entropy, a process that is further prolonged as the number of particles increases. In addition, we observe that the maximum Lyapunov exponent decays as a power–law with respect to the system size, indicating "integrable-like" behaviour in the thermodynamic limit. Finally, we give an analytic upper estimate for the growth of the maximum Lyapunov exponent in terms of the energy.

1. Introduction

Ergodicity-breaking and long-term stability are frequent phenomena in many-body Hamiltonian systems. There are various forms of non-equilibrium states that appear in such systems, such as the formation of metastable states, energy localisation, synchronisation, etc. These features are often accompanied by a weaker form of chaos, manifested by very low or vanishing Lyapunov exponents. Within many-body Hamiltonian systems, those involving long-range forces have an even more perplexed and enigmatic behaviour in terms of out-of-equilibrium long-lasting states.

In systems with long-range interactions (LRI), such as the Mean-Field Hamiltonian (MFH) [1,2] and the Fermi-Pasta–Ulam-Tsingou model with long-range interactions (FPUT-LRI) [3–6], chaoticity wanes by increasing the number of particles N, whilst the specific energy $\epsilon = E/N$ is kept constant (E is the total energy of the Hamiltonian). This property is intriguing and raises several questions about what happens in the thermodynamic limit of the models. These two systems share a common feature: they are translationally invariant.

There is a notable interest towards this direction in recent years; various works study in-depth FPUT models with LRI and their dynamical properties [7–11], as well as "realistic" versions of FPUT models, such as the ionic-crystal model, also called "the modern form of the FPU problem" [12,13]. Generally, it is understood that some models with LRI are more perplexed, whilst less chaotic, compared to their nearest-neighbour counterparts. This is also reflected in the statistical behaviour of the system. By examining the probability density functions (PDF) of the momenta of such models, it has been observed that these PDFs deviate from the classical Boltzmann–Gibbs (BG) thermostatistical description [14–19]. For example, there have been numerous cases where quasi-stationary states (QSS) form long-lived q-Gaussian momenta PDFs [3,12,18], described by non-extensive statistical mechanics and Tsallis entropy [16].

Recently, these studies were extended to Hamiltonian lattices without translational invariance [20], such as the Klein–Gordon (KG) model and its dispersionless variant, referred to by Gorbach and Flach as "a system with nonlinear and nonlocal dispersive terms" [21]. These two models are 1D lattices with nearest-neighbour interactions and on-site potentials that support the emergence of discrete breathers [22,23], namely, spatially localised (usually exponential) and time-periodic solutions. The main difference between these two models is that the latter exhibits stronger and more persistent localisation properties due to nonlinearity in dispersion. This difference leads to the formation of compactons, i.e. discrete breathers with compact support in this type of models [21,24–29].

When long-range interactions are introduced, the dynamics of the KG and dispersionless KG models undergo significant changes: the maximum Lyapunov exponent decreases with increasing N [20]. This

* Corresponding author.
E-mail address: canton@essex.ac.uk (C.G. Antonopoulos).

https://doi.org/10.1016/j.physd.2024.134432
Received 17 June 2024; Received in revised form 3 October 2024; Accepted 9 November 2024
Available online 19 November 2024

behaviour is similar to that observed in models with translational invariance, such as the MFH and FPUT-LRI systems. An open question remains as to whether these systems exhibit integrable-like and non-ergodic behaviour in the thermodynamic limit.

The paper is organised as follows: In the introduction 2 we discuss the Hamiltonian formalism of a dispersionless mean-field model of N globally coupled particles and its strong localisation properties which result to a variety of special solutions. Section 3 is devoted to the study of the Lyapunov exponent and its dependence on the energy 3.1, where we provide an analytic upper estimate for the growth of the maximum Lyapunov exponent as a function of the energy. Our study extends to the maximum Lyapunov exponent's dependence on the system size 3.2, which indicates organised behaviour in the thermodynamic limit. In Section 4 we analyse the path to thermalisation by computing the probability density distributions of the system's momenta and examining their gradual convergence to a Gaussian distribution within the framework of non-extensive statistical mechanics and Tsallis entropy. Finally, the paper closes with the conclusions section in 5.

2. The model

In this context, we examine the dispersionless mean-field Hamiltonian of N globally coupled particles, described by

$$H=\sum_{n=1}^{N}\left[\frac{1}{2}p_n^2+V(x_n)+\frac{1}{2\tilde{N}}\sum_{m=1}^{N}W(x_m-x_n)\right]=E, \tag{1}$$

where x_n is the displacement of the nth particle from its equilibrium position, p_n its conjugate momentum and E the total (constant) energy of the system. Within this framework, the expressions for the on-site potential V and the potential of all-to-all interactions W are given by

$$V(x_n)=\frac{1}{2}x_n^2+\frac{1}{4}x_n^4, \tag{2}$$

and

$$W(x_m-x_n)=\frac{1}{4}(x_m-x_n)^4, \tag{3}$$

respectively. Furthermore, periodic boundary conditions $x_{N+n}=x_n$ and $p_{N+n}=p_n$, $n=1,\dots,N$ have been considered. The divisor $\tilde{N}=N-1$ in the Hamiltonian (1) is necessary to ensure that the Hamiltonian H remains an extensive thermodynamic quantity. The corresponding equations of motion are given by

$$\ddot{x}_n=-x_n-x_n^3-\frac{1}{\tilde{N}}\sum_{m=1}^{N}(x_n-x_m)^3,\quad n=1,\dots,N. \tag{4}$$

This is a mean-field model with very strong energy localisation properties due to the absence of linear coupling terms. Here, the network of particle interactions is global and nonlinear. As we stated in the introduction, the nearest neighbour version of this model, with nonlinear dispersion terms

$$W(x_{n+1}-x_n)=\frac{1}{4}(x_{n+1}-x_n)^4$$

and the presence of an on-site potential, contributes to the formation of compactons [21,26,27]. In [21], it was shown that such solutions do exist even when the interactions extend from nearest neighbours to distance decaying forces. By extending the interactions of the model globally, with each particle interacting with all others in the system, as described in (1), the present paper aims to investigate the effect of non-topological maximal-range interactions on the dynamical and statistical characteristics of the mean field model.

Here, we numerically integrated the equations of motion of Hamiltonian (1) numerically, using the 4th order Yoshida's symplectic integrator [30]. In our simulations, we set the integration time step to $\tau=0.02$, a value chosen to maintain the relative energy error within an acceptable range

$$E_r=\left|\frac{E-E^{num}}{E^{num}}\right|\approx 10^{-6},$$

where E^{num} denotes the energy of Hamiltonian (1), computed along the numerical solution for all x_n and p_n.

2.1. Special solutions and localisation

The uniform interactions among the oscillators, in the absence of linear resonances, create suitable conditions for the emergence of various special low-dimensional solutions to the system (1). This interesting characteristic appears when a single or a packet of particles are initially excited, with their initial energy remaining localised on them at all times.

In Fig. 1(a), we show that the dynamics of a single-site excitation ($n=0$ particle) is well-described by an undamped Duffing equation

$$\ddot{x}_0=-x_0-x_0^3-(x_0-x_n)^3 \tag{5}$$

where x_n, $n\neq 0$, are negligible since they start by zero initial conditions and satisfy

$$\ddot{x}_n=-x_n-x_n^3-\frac{1}{\tilde{N}}(x_n-x_0)^3$$

for a rather large $\tilde{N}$ (see also [20]).By using Poincaré–Lindstedt series, we find that for $x_0(0)=0$, $\dot{x}_0(0)=A_0$, $A_0\ll 1$, Duffing Eq. (5) gives rise to periodic solutions of the form

$$x_0(t)=a\sin(\omega t),\ a=\frac{A_0}{\omega},\ \omega=1+\frac{3a^2}{4}. \tag{6}$$

In Fig. 1(a), we show the numerical solution of the system (4) for $N\gg 1$, when a single site is initially excited ($x_0(0)=0$, $\dot{x}_0(0)=0.5$), as well as its agreement with the estimate (6) derived from the Poincaré-Lindstedt series.

This property extends to multi-site excitations of $s\ll N$ particles, where the entire system (4) can be effectively represented by a reduced system of s uncoupled Duffing oscillators (5). This phenomenon arises from the uniform manner in which the oscillators interact. To test this argument numerically, we consider the excitation of a packet of $s=50$ consecutive sites of the system (4) with $N=1024$. Fig. 1(b),(c) show the solutions of $n=-5$ and $n=5$ sites, as well as the approximated solutions $x_{-5}(t)=0.318\sin(1.076t)$ and $x_5(t)=0.259\sin(1.05t)$ derived by Poincaré-Lindstedt series with initial velocities $\dot{x}_{-5}(0)=-0.343$ and $\dot{x}_5(0)=0.272$, respectively.

On the lack of energy spreading for these two solutions, we calculate numerically the evolution of the *normalised on-site energies*

$$\tilde{E}_n=\frac{E_n}{\tilde{E}}, \tag{7}$$

where

$$E_n=\frac{1}{2}\left(p_n^2+x_n^2+\frac{1}{2}x_n^4\right)\ \text{and}\ \tilde{E}=\sum_{n=1}^{N}E_n. \tag{8}$$

after (a) single and (b) multi-site excitations.

In Fig. 2(a),(b), we show the evolution of the normalised on-site energies $\tilde{E}_n$ (7) for $s=1$ and $s=50$ initially excited particles, respectively. Panels (a) and (b) show that the energy remains localised only to the initially excited particles with a nearly complete absence of diffusion to the rest sites. This means that the number of excited sites $s\ll N$ is practically the effective degrees of freedom of the system (4).

These strong localisation properties require further investigation when all particles are excited. We do not exclude the possibility of the existence of adiabatic invariants, as it occurs in other near-integrable systems like the FPUT model [31,32] and KG chain [33,34].

3. The maximal Lyapunov exponent

In this section, we analyse the chaotic behaviour of the mean-field model (1) for generic initial data. Particularly, we study the dependence of the maximal characteristic Lyapunov exponent λ on both system size and total energy. We also discuss the properties of λ across a wide range of energy values, as well as λ's asymptotic behaviour as the system approaches the thermodynamic limit.

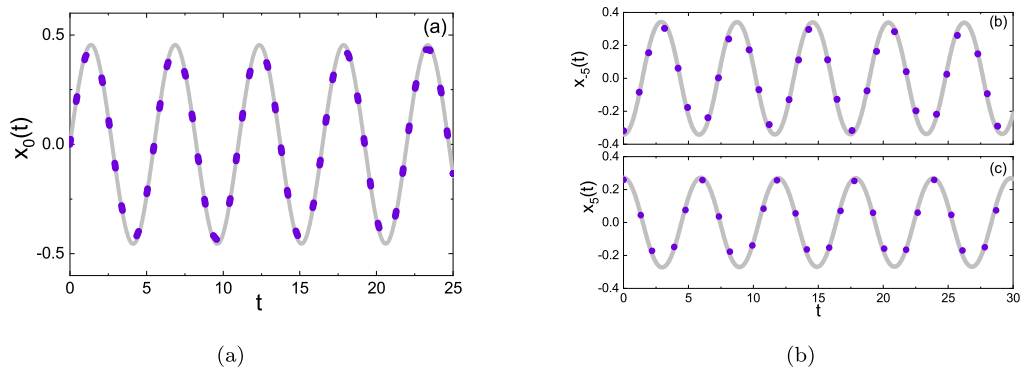

Fig. 1. The numerical solution of the system (4) with $N = 1024$ particles (a) for a single-site excitation and (b) for an excitation of a packet of $s = 50$ consecutive sites around the central site $n = 0$. This panel shows the numerical solution of the particles $n = -5$, $n = 5$ (grey curve). In both panels the blue dots represent the approximated solution derived from the Poincaré-Lindstedt series.

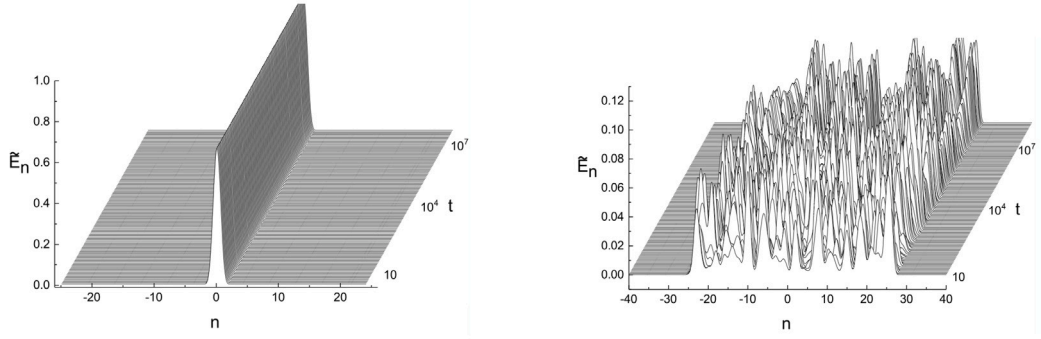

Fig. 2. The normalised on-site energies $\tilde{E}_n$ of system (4), where $N = 256$ (a) for a single-site ($s = 1$) excitation at $n = 0$ and (b) for an excitation of a packet of $s = 50$ consecutive sites around the central site $n = 0$.

As is well known, the computation of the Lyapunov exponents requires integrating the variational equations

$$\dot{\boldsymbol{\xi}} = [J \cdot D^2 H(\mathbf{x}(t), \mathbf{p}(t))] \cdot \boldsymbol{\xi}, \tag{9}$$

where $\boldsymbol{\xi} = (\delta\mathbf{x}, \delta\mathbf{p})$ is a vector in the tangent space of the phase space of system (1), J is the standard symplectic matrix and D^2H is the Hessian of the Hamiltonian H, evaluated along the reference orbit $(\mathbf{x}(t), \mathbf{p}(t))$. The vector $\boldsymbol{\xi}$ measures the distance growth of two nearby orbits of system (1). The system (9) yields from the time-dependent Hamiltonian system

$$\mathcal{H} = \sum_n \left[\frac{1}{2}(\delta\mathbf{p_n})^2 + \frac{\partial^2 V}{\partial x_n^2}(\delta\mathbf{x_n})^2 + \frac{1}{2\tilde{N}} \sum_m \frac{\partial^2 W}{\partial x_n \partial x_m} \delta\mathbf{x_n}\delta\mathbf{x_m} \right]. \tag{10}$$

The numerical approximation of the maximal Lyapunov exponent λ entails the calculation of a finite-time Lyapunov exponent $\lambda(T) = \frac{1}{T} \ln \frac{\|\xi(T)\|}{\|\xi(0)\|}$, which is expected to stabilise at the asymptotic λ value

$$\lambda = \lim_{t\to\infty} \frac{1}{t} \ln \frac{\|\boldsymbol{\xi}(t)\|}{\|\boldsymbol{\xi}(0)\|}$$

after a transient time.

3.1. Energy dependence

Evaluating analytically the maximal Lyapunov exponent is a notoriously difficult task. It is worth mentioning the pioneer works [35–37] on approaching Hamiltonian chaos in the Fermi-Pasta–Ulam-Tsingou model by geometric means, such as estimating the curvature fluctuations along trajectories on a Riemannian manifold. This approach shows that such equations lead to a stochastic Hill's equation with a linear coefficient described by a Gaussian random process, with mean and variance related to Ricci's curvature. This method can be used to accurately evaluate the maximal Lyapunov exponent $\lambda(\varepsilon)$ for the FPUT-β model and its dependence on the specific energy $\varepsilon = E/N$: $\lambda(\varepsilon) \propto \varepsilon^2$ for $\varepsilon \to 0$ and $\lambda(\varepsilon) \propto \varepsilon^{1/4}$ for $\varepsilon \to \infty$. Many other papers emerged afterwards, with one of the most recent ones by Benettin at al. [38], who generalised it for FPUT type of models in the linear hierarchy. In [38], it was shown that at small energies, $\lambda(\varepsilon) \propto \varepsilon^3$ when the potential function $V(r)$, with $r = x_{n+1} - x_n$, is of order 5 and $\lambda(\varepsilon) \propto \varepsilon^4$ when $V(r)$ is of order 6.

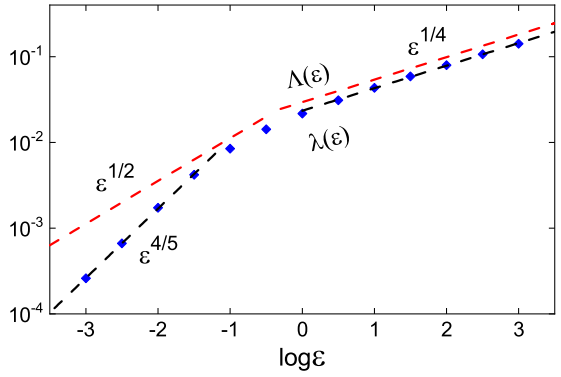

Fig. 3. Plot of the maximal Lyapunov exponents λ versus the specific energy ε for $N = 16384$ particles. Note that the scale in both axes is logarithmic and that, the black dash lines are fittings to the numerical Lyapunov exponent data and the two energy regimes correspond to different scaling laws: For small specific energies, $\lambda \propto \varepsilon^{4/5}$ and for larger specific energies, $\lambda \propto \varepsilon^{1/4}$. The red dashed line corresponds to the upper bound estimation $\Lambda(\varepsilon)$.

Building upon these findings, we investigate the tangent dynamics (9) for the mean field model (1), with more details given in Appendix. The matrix $A = D^2(V + W)$ in the system of second order differential equations

$$\ddot{\boldsymbol{\delta}}\mathbf{x} = -A(t) \cdot \boldsymbol{\delta}\mathbf{x}, \tag{11}$$

has two types of elements; $a_{nm} = -\frac{3}{N}(x_n - x_m)^2$ are all non-diagonal entries and $a_{nn} = 1 + 3x_n^2 + \frac{3}{N}\sum_{m=1}^{N}(x_n - x_m)^2$ are the entries on the diagonal. A diagonalisation of system (11) yields a set of stochastic Hill's equations, where each one is of the form

$$\frac{d^2\psi}{dt^2} = -\kappa(t)\psi, \tag{12}$$

with $\kappa(t)$ representing an eigenvalue of $A = D^2(V + W)$ at time t. Since each of $\kappa(t)$ can represent a stochastic process, estimating the size of ψ or predicting the asymptotic behaviour of the length of $\boldsymbol{\xi}(t)$ poses considerable difficulty, hence a straight-forward evaluation of the Lyapunov exponent is nearly impossible.

Our objective here is to gain insight into the spectrum of eigenvalues. To this end, we consider micro-canonical averages $\langle\cdot\rangle$, which simplify $A = D^2(V + W)$ to the symmetric matrix $\langle A\rangle$ containing only two types of elements a (off-diagonal) and b (diagonal), where $a = \langle a_{nm}\rangle = -\frac{6}{N}\langle x_n^2\rangle$ for all $n, m = 1, \dots, N$ with $n \neq m$, and $b = \langle a_{nn}\rangle = 1 + 9\langle x_n^2\rangle$. We note that all non-diagonal entries a vanish as $N \to \infty$, hence in the thermodynamic limit, this matrix becomes the diagonal bI. Instead, for a finite $N \gg 1$ the simplified matrix $\langle A\rangle$ has two types of eigenvalues

$$\kappa_1 = b - a \simeq 1 + 9\langle x_n^2\rangle \text{ and } \kappa_2 = b + \tilde{N}a \simeq 1 + 3\langle x_n^2\rangle.$$

Since both eigenvalue types are approximated by quantities of the same form, i.e. $1 + c\langle x_n^2\rangle$ for some constant c, a rough estimate for κ is that it scales with the mean squared particle displacement like $\kappa \propto \langle x_n^2\rangle$. On the other hand, we know that as $\varepsilon \to 0$, it is $\langle x_n^2\rangle \propto \varepsilon$, while as $\varepsilon \to \infty$, it yields that $\langle x_n^2\rangle \propto \varepsilon^{1/2}$. This can be easily derived from the Hamiltonian (1), where the cut-off energy is about $\varepsilon \simeq 1$. Hence, we conclude that κ scales with the specific energy as

$$\kappa(\varepsilon) \propto \varepsilon^p, \tag{13}$$

where $p = 1$ at low energies and $p = 1/2$ at higher. We also anticipate a similar tendency for the maximal Lyapunov exponent, λ increasing at varying rates in the low and high energy limits, with a distinct transition occurring around $\varepsilon \simeq 1$.

Despite the power-law growth estimation (13) of the κ coefficient, obtaining an analytic approximation for the solution to Hill's equation remains challenging. This trend is anticipated not only due to the presence of a dense web of resonances [39], but also because of the complexity involved in evaluating the fluctuations of $\langle x_n^2\rangle$. These fluctuations are expected to offer a more precise estimation of how λ depends on κ. Such a study is deferred to a future work. In this study, we focus on a conjecture about dependence of the Lyapunov exponent on $\kappa(\varepsilon)$, which naturally arises with the increase in specific energy ε.

Let $\Lambda(\varepsilon)$ be an upper bound for the maximal Lyapunov exponent $\lambda(\varepsilon)$. Considering Hill's Eqs. (12), this upper bound is expected to vary proportionally to the square root of the exponent of solution's most unstable direction, as if the solution of (12) were purely exponential without periodicity. In other words,

$$\lambda(\varepsilon) \leq \Lambda(\varepsilon), \tag{14}$$

where

$$\Lambda(\varepsilon) \propto \sqrt{\kappa(\varepsilon)}, \tag{15}$$

which imply $\Lambda(\varepsilon) \propto \varepsilon^{1/2}$ for $\varepsilon \ll 1$ and $\Lambda(\varepsilon) \propto \varepsilon^{1/4}$ for $\varepsilon \gg 1$.

We proceed to numerically investigate the dependence of the maximal Lyapunov exponent $\lambda(\varepsilon)$, for specific energies as low as 0.001 up to values reaching 1000, and compare these findings with the upper bound estimate $\lambda(\varepsilon)$. Over the span of seven orders of magnitude, the behaviour of λ has been evaluated for a system with $N = 16384$ particles. The initial conditions are of waterbag-type, i.e. the momenta have been randomly extracted from a uniform distribution and initial positions are all set to zero.

In Fig. 3, we observe that λ monotonically increases with respect to the specific energy ε, however at different speeds. In particular, the initial steep rise of λ follows the power-law growth $\lambda(\varepsilon) \propto \varepsilon^{4/5}$ in terms of ε, which slows down to $\lambda(\varepsilon) \propto \varepsilon^{1/4}$ beyond the turning point $\varepsilon_c \approx 0.1$ for $N = 16384$. These results of Fig. 3 compare nicely with the upper bound $\Lambda(\varepsilon)$ in (14), providing a very good prediction for the growth of the maximal Lyapunov exponent at high energies.

3.2. A declining chaos

In Hamiltonian models with long-range interactions it has been pointed out that chaos declines with the system size [1–6]. This phenomenon is known to occur when the interacting forces have a sufficiently long range, whereas models with nearest-neighbour interactions, such as the FPUT model, do not exhibit noticeable dynamical and statistical changes by increasing N and keeping the energy density ε constant (ε above a critical threshold).

In the case of the dispersionless mean-field model (1), we numerically study the maximal Lyapunov exponent λ for increasing system sizes $N = 64, 128, \dots, 16384$. We perform four sets of experiments for the energies $\varepsilon = 0.01$, 0.1, 1 and 10, corresponding to consecutive orders of magnitude that spread from very low, intermediate to high. Our findings presented in Fig. 4(a) suggest that λ decays as $N^{-0.3}$ for each ε value and above a certain size threshold $N \approx 100$, indicating that this power-law behaviour is independent of the energy level. Moreover, the critical size inversely depends on the energy, meaning that smaller system sizes follow this power-law by increasing the energy.

In Fig. 4(b), we rescale the parallel fitting lines of Fig. 4(a) into one single line, given by

$$\log\tilde{\lambda} = -0.3179 \log N - 0.32. \tag{16}$$

This scaling law is derived from Fig. 4(a) data by absorbing the energy dependence reported in Section 3.1, where it was found that $\lambda(\varepsilon) \propto \varepsilon^{-c}$ with $c = 4/5$ for $\varepsilon < 1$ and $c = 1/4$ for $\varepsilon > 1$. Since

$$\lambda(\varepsilon, N) \propto \varepsilon^c N^{-0.3}, \tag{17}$$

we considered

$$\tilde{\lambda}(N) = \lambda(\varepsilon, N)\varepsilon^{-c}$$

for the c values as given above, which removes this energy dependence.

These data suggest a tendency towards organised dynamical behaviour in the thermodynamic limit. Our findings indicate that mean-field type of interactions lead to an overall decline in the system's chaotic ($\tilde{\lambda} \propto N^{-0.3}$) as N increases, occurring independently of the energy level. However, the mechanism by which this chaotic decline emerges from the variational Eqs. (9) remains an open question.

4. Statistical analysis

In Section 3.2, we have seen that for the Hamiltonian with long-range interactions (1), chaoticity declines with the system size N, in the sense that the maximal Lyapunov exponent λ decreases as a function of ε and N, but is still positive. This happens mostly when the interacting forces are above a certain range.

Here, we complement our study in Section 3.2 and focus on the statistical behaviour of Hamiltonian (1) for a large-enough specific energy ε and increasing system-sizes N, to see whether the system moves towards equipartition of energy in the thermodynamic limit. We do this by looking at the statistical properties of its trajectories in the context of non-extensive Statistical Mechanics [16].

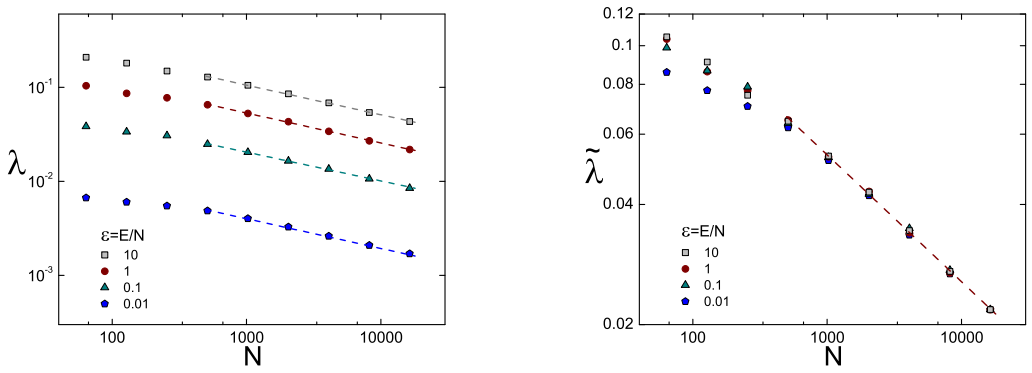

Fig. 4. (a) The maximal Lyapunov exponents λ versus N at various levels of the specific energy, i.e. $\varepsilon = 0.01$, 0.1, 1 and 10. (b) The rescaled values $\tilde{\lambda}$ of the maximal Lyapunov exponent λ in panel (a) according to $\tilde{\lambda}(\varepsilon, N) \approx 0.48 N^{-0.3}$. Note that the scale in all axes is logarithmic.

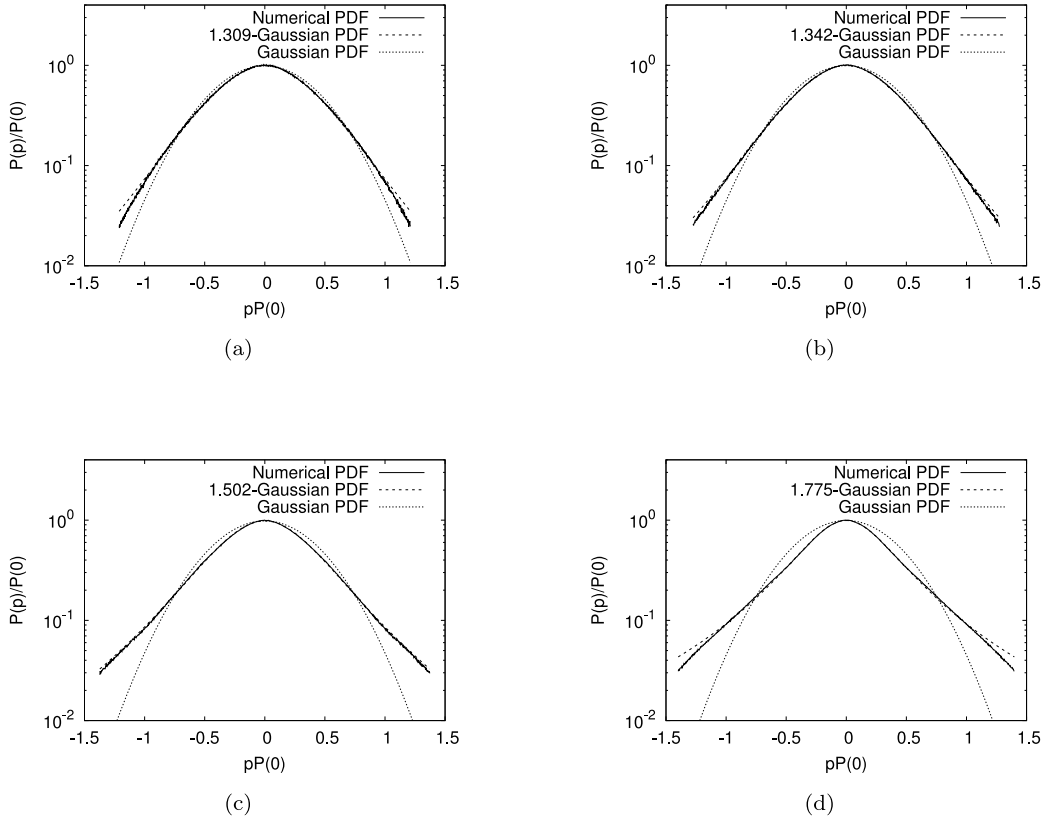

Fig. 5. PDFs for different N at time $t = 1.5 \times 10^6$: Plot of the PDF for (a) $N = 512$, where $q \approx 1.309$, (b) $N = 1024$, where $q \approx 1.342$, (c) $N = 2048$, where $q \approx 1.502$ and (d) $N = 4096$, where $q = 1.775$. In all cases, $\varepsilon = 10$. Note that all horizontal axes are in linear scale and all vertical axes in logarithmic scale. Note also that solid curves are the plots of the numerical PDFs, dashed curves are the plots of the best-fits to the numerical PDFs and dotted curves are the plots of Gaussian PDFs for reference ($q = 1$).

Particularly, we look at the time evolution of the entropic index q of Hamiltonian (1) for the specific energy $\varepsilon = 10$ and for increasing N up to $N = 4096$ particles. The entropic index q is associated with the q-Gaussian probability density function (PDF) [16]

$$\mathrm{P}(x) = \alpha\left(1 + \beta(q-1)x^2\right)^{\frac{1}{1-q}}, \tag{18}$$

where α is a normalisation constant and β an arbitrary parameter. Eq. (18) is a generalisation of the well-known Gaussian PDF, since in the limit $q \to 1$, $\mathrm{P}(x)$ becomes the Gaussian PDF [16]. Moreover, it has been shown in [19] that the q-Gaussian distribution is normalised when

$$\sqrt{\beta} = \alpha\sqrt{\pi}\frac{\Gamma\left(\frac{3-q}{2(q-1)}\right)}{(q-1)^{\frac{1}{2}}\Gamma\left(\frac{1}{q-1}\right)},$$

where Γ is the Euler Γ function and $1 < q < 3$.

As we saw in Fig. 4(a), the maximal Lyapunov exponent λ decreases to zero for increasing N, following Eq. (17), where $c = 1/4$ as $\varepsilon = 10 > 1$,

$$\lambda(\varepsilon, N) \propto \varepsilon^c N^{-0.3}.$$

This means λ attains positive but very small values as N increases.

We use the numerical solutions to the equations of motion of Hamiltonian (1) to compute the PDF of the dynamics to estimate the entropic index q in time. The index q in Eq. (18) is connected with the Tsallis entropy [16]. Systems characterised by the Tsallis entropy are said to lie at the "edge of chaos" and are significantly

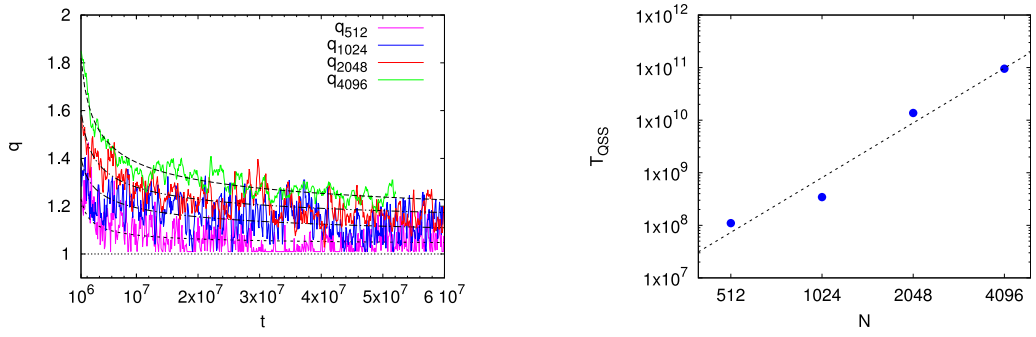

Fig. 6. Plot of the entropic index q in time and T_{QSS} versus N. Panel (a): Plot of the entropic index q in time for different N (denoted by the subscripts). The black-dash curves are given by Eq. (19) and are the best-fit curves to the data in colour for $N = 512$, 1024, 2048 and 4096. Panel (b): Plot of T_{QSS} versus N, where the dash black line is the best fit to the blue points (discussed in the text), using Eq. (20). Note that $\epsilon = 10$ and that the scale in all axes is logarithmic.

different from Boltzmann–Gibbs systems, in the sense that their entropy is non-additive and generally, non-extensive [16].

We start by using as a probe for the computation of the PDFs, the p_i components of the solutions to Hamiltonian (1) and define a range of values in the interval $[-10, 10]$ on the horizontal axis of the PDF plot, partitioning it in 1000 bins. We have made sure this interval contains the whole PDF for $\epsilon = 10$ and all integration times. We then count how many p_i fall into each bin at multiples of $\tau = 5$ for $t \geq 10^5$ to avoid introducing correlation effects in the computations. We compute the resulting PDFs at multiples of $t = 10^5$ by dividing the counts in each bin by the total number of counts over all bins (i.e., we compute the probability p of occurrences within the ith bin, where $i = 1, \ldots, 1000$). We plot $pP(0)$ on the horizontal axis of the PDF plot and $P(p)/P(0)$ on the vertical axis, where $P(0)$ is the value of the PDF at $p = 0$ (i.e., at the centre of the PDF). This results in a normalised PDF (18) with a maximum at 1 on the vertical axis (see for example the PDFs in Fig. 5). The counts are reset after the computation of the PDFs at multiples of $t = 10^5$, which means we compute PDFs for times between time intervals $[10^5, 2 \times 10^5]$, $[2 \times 10^5, 3 \times 10^5]$, etc., so that we do not carry over information from previous time windows. After computing the numerical PDFs at the end of these time windows, we fit them numerically with Eq. (18) to estimate the entropic index q, making sure the area under them is equal to 1.

We plot examples of these numerical PDFs (solid black curves), q-Gaussians (dashed black curves) and Gaussian (dotted black curves) PDFs in Fig. 5 (for details, see caption in Fig. 5) at $t = 1.5 \times 10^6$. Panel (a) shows the output of this analysis for a numerical PDF computed for $N = 512$ with $q \approx 1.309$, panel (b) for $N = 1024$ and $q \approx 1.342$ and panel (c) for $N = 2048$ and $q \approx 1.502$. Finally, panel (d) shows the numerical PDF that results from the system with $N = 4096$, where $q \approx 1.775$. These results show that at $t = 1.5 \times 10^6$, the dynamics become more weakly chaotic as N increases.

We extend the results of this analysis in Fig. 6, where we plot the evolution of the entropic index q for specific energy $\epsilon = 10$ and $N = 512$ (magenta), 1024 (blue), 2048 (green), 4096 (red) in panel (a). We see that q decreases in time towards $q = 1$ of the Gaussian PDF, following the power-law

$$q_N(t) = a_N + \frac{b_N}{t^{c_N}}, \tag{19}$$

where the values of a_N, b_N and c_N are reported in Table 1. Fig. 7 in the Appendix shows the weighted sum of squares of residuals (WSSR) resulting from the numerical fits of the coloured curves in panel (a) with function (19).

This power-law was obtained by fitting the curves with function (19). These results indicate that as the time it takes for the system to converge to $q = 1$ increases as N increases, the dynamics of Hamiltonian (1) undergoes a quasi-stationary state (QSS) that lasts for longer and longer as N increases, characterised by weakly chaotic dynamics. We looked into this more in panel (b) in Fig. 6. Particularly, we estimated the time $T_{\text{QSS}}(N)$ it takes for the dynamics of the system for different N to reach a q value of 1% of a_N, as $q_N(t)$ in Eq. (19) is monotonically decreasing and converges to a_N as $t \to \infty$. In Fig. 6(b), we plot the estimated time $T_{\text{QSS}}(N)$ for $q_N(t)$ to become $1.01a_N$ versus N, depicted by the blue points. These times are approximations of the duration of the QSS (T_{QSS}), before the dynamics can be described by q close to 1. The plot confirms T_{QSS} is increasing as a function of N, according to

$$T_{\text{QSS}}(N) = aN^b, \tag{20}$$

where $a \approx 0.031$ and $b \approx 3.46$, obtained by fitting the blue points in panel (b) with Eq. (20).

Table 1
Parameter values a_N, b_N and c_N of Eq. (19) for a range of N values.

N	a_N	b_N	c_N
512	1.033	1130.288	0.627
1024	1.069	956.450	0.580
2048	1.075	146.806	0.408
4096	1.062	129.681	0.372

While in this paper we included only the case of $\epsilon = 10$, preliminary simulations indicate that the value of q increases at higher energies. This phenomenon is attributed to the non-linear terms gathering most of the energy, which enhances the occurrence of rare events and results in more pronounced tails in the distributions. It is worth mentioning that this behaviour is consistent with the maximal Lyapunov exponent, which decreases as N increases.

These results, combined with the results in Section 3.2 about the declining of the maximal Lyapunov exponents, show that as N increases, the length of the QSS increases and that chaoticity decreases. This might be evidence that in the thermodynamic limit, the dynamics of Hamiltonian (1) is weakly chaotic, and that equipartition of energy is pushed further in time as N increases, making it more difficult to observe.

5. Conclusions

The primary objective of this study was to explore the impact of nonlinear long-range interactions on the dynamical and statistical properties of many-body Hamiltonian models with on-site potentials. In numerical simulations with a few particles excited, the solution of the system remained constrained in lower-dimensional manifolds of the phase space. Such systems with long-range interactions are promising candidates for investigating diverse localised solutions and deserve a further study.

$$A = \begin{pmatrix} 1+3x_1^2+\frac{3}{N}\sum_m (x_1-x_m)^2 & -\frac{3}{N}(x_1-x_2)^2 & \dots & -\frac{3}{N}(x_1-x_N)^2 \\ -\frac{3}{N}(x_1-x_2)^2 & 1+3x_2^2+\frac{3}{N}\sum_m (x_2-x_m)^2 & \dots & -\frac{3}{N}(x_2-x_N)^2 \\ \vdots & \vdots & \vdots & \ddots \\ -\frac{3}{N}(x_1-x_N)^2 & -\frac{3}{N}(x_2-x_N)^2 & \dots & 1+3x_N^2+\frac{3}{N}\sum_m (x_N-x_m)^2 \end{pmatrix}.$$

Box I.

For generic initial conditions, we estimated the maximal Lyapunov exponent's scaling laws, describing its increase with respect to the system's energy. This method works well at high energies and yields $\lambda(\varepsilon) \propto \varepsilon^{1/4}$. We also observed a dynamical regularisation towards the thermodynamic limit. This regularisation is characterised by a power-law decay of $\lambda\ N^{-\mu}$, where $\mu \simeq 0.3$, suggesting a milder form of chaos as N approaches infinity. These findings are further supported by the non-trivial statistical patterns observed in the corresponding PDFs of the momenta of the system. These PDFs are well-fitted by q-Gaussian distributions and show that as N increases, the time-length of the QSS increases too. This combined with our results that chaoticity decreases as N increases, might suggest that in the thermodynamic limit, the dynamics of Hamiltonian (1) is weakly chaotic, and that equipartition of energy is pushed further in time as N increases, making it difficult to observe.

Such phenomena are encountered more often in models with long-range interactions, such as the Mean-Field model and FPUT with long-range forces. Hence further exploration and classification of different systems that exhibit similar behaviours and their implications is required but would be intriguing.

CRediT authorship contribution statement

H. Christodoulidi: Writing – review & editing, Writing – original draft, Visualization, Validation, Software, Methodology, Investigation, Formal analysis, Conceptualization. **Ch. G. Antonopoulos:** Writing – review & editing, Writing – original draft, Visualization, Validation, Software, Resources, Methodology, Investigation, Formal analysis.

Declaration of competing interest

The authors declare that they have no known competing financial interests or personal relationships that could have appeared to influence the work reported in this paper.

Acknowledgements

The authors acknowledge interesting discussions with Prof. C. Tsallis. They also acknowledge the use of the High Performance Computing Facility (Ceres) and its associated support services at the University of Essex, UK in the completion of this work.

Appendix

Variational equations and maximal Lyapunov exponent

The matrix $A = D^2(V + W)$ in the system of variational equations

$$\ddot{\delta}\mathbf{x} = -A(t) \cdot \delta\mathbf{x} \tag{21}$$

of system (4) is given by (see the equation in Box I).

We use the system of variational Eqs. (21) (tangent system) to calculate the maximal Lyapunov exponent [40], according to Benettin et al. [41].

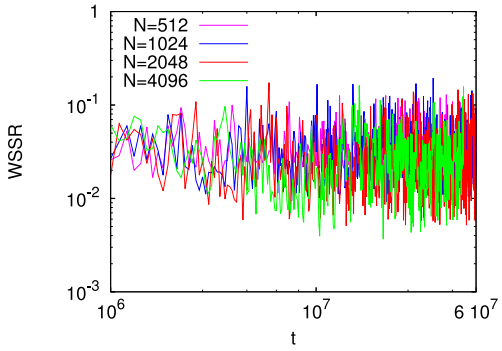

Fig. 7. Plot of WSSR in time for different N, resulting from best-fitting the data in panel (a) in Fig. 6 with Eq. (19). Note that the scale in both axes is logarithmic.

Statistical analysis and goodness-of-fit

Fig. 7 shows the weighted sum of squares of residuals (WSSR) resulting from the numerical fits of the coloured curves in panel (a) in Fig. 6 with function (19). Even though these curves exhibit large fluctuations, WSSR is bounded between 10^{-1} and 10^{-2} for all N considered, and the fittings follow the trends of the coloured curves. Hence they were used in the subsequent analysis.

Data availability

Data will be made available on request.

References

[1] V. Latora, A. Rapisarda, S. Ruffo, Lyapunov instability and finite size effects in a system with long-range forces, Phys. Rev. Lett. 80 (1998) 692.
[2] C. Anteneodo, C. Tsallis, Breakdown of exponential sensitivity to initial conditions: Role of the range of interactions, Phys. Rev. Lett. 80 (1998) 5313.
[3] H. Christodoulidi, C. Tsallis, T. Bountis, Fermi–Pasta–Ulam model with long-range interactions: Dynamics and thermostatistics, Europhys. Lett. 108 (2014) 40006.
[4] H. Christodoulidi, T. Bountis, C. Tsallis, L. Drossos, Dynamics and statistics of the Fermi–Pasta–Ulam β-model with different ranges of particle interactions, J. Stat. Mech. 123206 (2016).
[5] D. Bagchi, C. Tsallis, Sensitivity to initial conditions of a -dimensional long-range-interacting quartic Fermi–Pasta–Ulam model: Universal scaling, Phys. Rev. E 93 (6) (2016) 062213.
[6] D. Bagchi, C. Tsallis, Fermi–Pasta–Ulam–Tsingou problems: Passage from Boltzmann to q-statistics, Phys. A 491 (2018) 869–873.
[7] G. Miloshevich, J.P. Nguenang, T. Dauxois, R. Khomeriki, S. Ruffo, Instabilities and relaxation to equilibrium in long-range oscillator chains, Phys. Rev. E 91 (2015) 032927.
[8] G. Miloshevich, J.P. Nguenang, T. Dauxois, R. Khomeriki, S. Ruffo, Traveling solitons in long-range oscillator chains, J. Phys. A 50 (2017) 12LT02.
[9] G.N.B. Chendjou, J.P. Nguenang, A. Trombettoni, T. Dauxois, R. Khomeriki, S. Ruffo, Fermi–Pasta–Ulam chains with harmonic and anharmonic long-range interactions, Commun. Nonlinear Sci. Numer. Simul. 60 (2018) 115–127.
[10] S. Iubini, S. Lepri, R. Livi, L. Casetti, Heat transport in oscillator chains with long-range interactions coupled to thermal reservoirs, Phys. Rev. E 97 (3) (2018) 032102.

[11] P. Di Cintio, S. Iubini, S. Lepri, R. Livi, Equilibrium time-correlation functions of the long-range interacting Fermi–Pasta–Ulam model, J. Phys. A 52 (27) (2019) 274001.
[12] A. Carati, L. Galgani, F. Gangemi, Approach to equilibrium via tsallis distributions in a realistic ionic-crystal model and in the FPU model, Eur. Phys. J. Spec. Top. 229 (2020) 743–749.
[13] F. Gangemi, R. Gangemi, A. Carati, L. Galgani, Thermal fluctuations in a realistic ionic-crystal model, Phys. A 586 (2022) 126463.
[14] C. Tsallis, Possible generalization of Boltzmann–Gibbs statistics, J. Stat. Phys. 52 (1988) 479–487.
[15] M. Gell-Mann, C. Tsallis (Eds.), Nonextensive Entropy - Interdisciplinary Applications, Oxford University Press, New York, 2004.
[16] C. Tsallis, Introduction to Nonextensive Statistical Mechanics - Approaching a Complex World, Springer, New York, 2009.
[17] C. Tsallis, An introduction to nonadditive entropies and a thermostatistical approach of inanimate and living matter, Contemp. Phys. 55 (2014) 179–197.
[18] L.J.L. Cirto, V. Assis, C. Tsallis, Influence of the interaction range on the thermostatistics of a classical many-body system, Phys. A 393 (2014) 286–296.
[19] S. Umarov, C. Tsallis, S. Steinberg, On a q-central limit theorem consistent with nonextensive statistical mechanics, Milan J. Math. 76 (2008) 307–328.
[20] H. Christodoulidi, A. Bountis, L. Drossos, The effect of long-range interactions on the dynamics and statistics of 1D Hamiltonian lattices with on-site potential, Eur. Phys. J. Spec. Top. 227 (2018) 563–573.
[21] A.V. Gorbach, S. Flach, Compactlike discrete breathers in systems with nonlinear and nonlocal dispersive terms, Phys. Rev. E 72 (2005) 056607.
[22] R.S. MacKay, S. Aubry, Proof of existence of breathers for time-reversible or Hamiltonian networks of weakly coupled oscillators, Nonlinearity 7 (1994) 1623.
[23] S. Flach, Obtaining breathers in nonlinear Hamiltonian lattices, Phys. Rev. E 51 (1995) 3579.
[24] P. Rosenau, J.M. Hyman, Compactons: Solitons with finite wavelength, Phys. Rev. Lett. 70 (1993) 564.
[25] P. Tchofo Dinda, T.C. Kofane, M. Remoissenet, Motion of compactonlike kinks, Phys. Rev. E 60 (1999) 7525.
[26] J.C. Comte, Exact discrete breather compactons in nonlinear Klein–Gordon lattices, Phys. Rev. E 65 (6) (2002) 067601.
[27] Y.S. Kivshar, Intrinsic localized modes as solitons with a compact support, Phys. Rev. E 48 (1993) R43–45.
[28] P. Maniadis, T. Bountis, Quasiperiodic and chaotic discrete breathers in a parametrically driven system without linear dispersion, Phys. Rev. E 73 (2006) 046211.
[29] S. Flach, Breathers on lattices with long range interaction, Phys. Rev. E 58 (4) (1998) R4116–R4119.
[30] H. Yoshida, Construction of higher order symplectic integrators, Phys. Lett. A 150 (5–7) (1990) 262–268.
[31] H. Christodoulidi, C. Efthymiopoulos, Stages of dynamics in the Fermi–Pasta–Ulam system as probed by the first Toda integral, Math. Eng. AIMS 1 (2) (2019) 359–377.
[32] T. Grava, A. Maspero, G. Mazzuca, A. Ponno, Diabatic invariants for the FPUT and toda chain in the thermodynamic limit, Comm. Math. Phys. 380 (2020) 811–851.
[33] A. Giorgilli, S. Paleari, T. Penati, Extensive adiabatic invariants for nonlinear chains, J. Stat. Phys. 148 (2012) 1106–1134.
[34] A. Giorgilli, S. Paleari, T. Penati, An extensive adiabatic invariant for the Klein–Gordon model in the thermodynamic limit, Ann. Henri Poincaré 16 (2015) 897–959.
[35] L. Casetti, R. Livi, M. Pettini, Gaussian model for chaotic instability of Hamiltonian flows, Phys. Rev. Lett. 74 (1995) 375–378.
[36] L. Casetti, C. Clementi, M. Pettini, Riemannian theory of Hamiltonian chaos and Lyapunov exponents, Phys. Rev. E 54 (1996) 5969–5984.
[37] M. Pettini, L. Casetti, M. Cerruti-Sola, R. Franzosi, E.G. Cohen, Weak and strong chaos in Fermi–Pasta–Ulam models and beyond, Chaos 15 (2005) 015106.
[38] G. Benettin, S. Pasquali, A. Ponno, The Fermi–Pasta–Ulam problem and its underlying integrable dynamics: An approach through Lyapunov exponents, J. Stat. Phys. 171 (2018) 521–542.
[39] H. Broer, C. Simó, Resonance tongues in Hill's equations: A geometric approach, J. Differential Equations 166 (2) (2000) 290–327.
[40] H. Christodoulidi, T. Bountis, L. Drossos, Numerical integration of variational equations for Hamiltonian systems with long range interactions, Appl. Numer. Math. 104 (2016) 158–165.
[41] G. Benettin, L. Galgani, A. Giorgilli, J.M. Strelcyn, Lyapunov characteristic exponents for smooth dynamical systems and for Hamiltonian systems; a method for computing all of them. Part 1: Theory, Meccanica 15 (1980) 9–20.